



Article

# Functionalized Activated Carbon Derived from Palm Kernel Shells for the Treatment of Simulated Heavy Metal-Contaminated Water

Rabia Baby <sup>1,2</sup>, Mohd Zobir Hussein <sup>1,\*</sup>, Zulkarnain Zainal <sup>1</sup> and Abdul Halim Abdullah <sup>1</sup>

<sup>1</sup> Material Synthesis and Characterization Laboratory, Institute of Advanced Technology, Universiti Putra Malaysia, Serdang 43400, Selangor, Malaysia; rabia.Shaikh@iba-suk.edu.pk (R.B.); zulkar@upm.edu.my (Z.Z.); halim@upm.edu.my (A.H.A.)

<sup>2</sup> Department of Education, Sukkur IBA University, Sukkur, Sindh 65200, Pakistan

\* Correspondence: mozobir@upm.edu.my

**Abstract:** Heavy metal contamination in water poses a great risk to human health as well as to the lives of other creatures. Activated carbon is a useful material to be applied for the treatment of heavy metal-contaminated water. In this study, functionalized activated carbon (FAC) was produced by the induction of nitro groups onto activated carbon using nitric acid. The resulting material was characterized in detail using the XRD, Raman, BET, FTIR, and FESEM techniques. The FAC was used for the treatment of heavy metal-contaminated water using different adsorption parameters, i.e., solution pH, contact time, adsorbent dosage and heavy metal ion concentrations, and these parameters were systematically optimized. It was found that FAC requires 90 min for the maximum adsorption of the heavy metal ions; Cr<sup>6+</sup>, Pb<sup>2+</sup>, Zn<sup>2+</sup> and Cd<sup>2+</sup>. The kinetic study revealed that the metal ion adsorption follows the pseudo-second-order. The Freundlich and Langmuir isotherms were applied to determine the best fitting adsorption isotherm models. The adsorption capacities were also determined for each metal ion.

**Keywords:** heavy metals; activated carbon; metal adsorption; water contamination; and water purification



**Citation:** Baby, R.; Hussein, M.Z.; Zainal, Z.; Abdullah, A.H.

Functionalized Activated Carbon Derived from Palm Kernel Shells for the Treatment of Simulated Heavy Metal-Contaminated Water.

*Nanomaterials* **2021**, *11*, 3133.

<https://doi.org/10.3390/nano11113133>

Academic Editor: George Z. Kyzas

Received: 6 April 2021

Accepted: 8 June 2021

Published: 20 November 2021

**Publisher's Note:** MDPI stays neutral with regard to jurisdictional claims in published maps and institutional affiliations.



**Copyright:** © 2021 by the authors. Licensee MDPI, Basel, Switzerland. This article is an open access article distributed under the terms and conditions of the Creative Commons Attribution (CC BY) license (<https://creativecommons.org/licenses/by/4.0/>).

## 1. Introduction

The industrialization has made life easier; unfortunately, at the same time, it has contributed significantly to environmental pollution, i.e., water pollution, soil pollution and air pollution [1–3]. Because of increased industrialization, clean and pure drinking water resources are becoming scarcer day by day. There are many sources of water contaminants; bacteria, viruses, organic compounds, organic dyes, and heavy metal ions such as cadmium, chromium, zinc, arsenic and mercury.

Heavy metal contaminants are non-biodegradable, causing immense risk to humans and other living creatures. These heavy metals accumulate in the body and harm health, such as through kidney damage, cancer, hepatitis, anemia, miscarriages, nephritic syndrome and encephalopathy, etc. [4–6]. There are various sources of heavy metals. Lead (Pb<sup>2+</sup>) enters into the environment from metal mining industries, lead-acid batteries, glass, paper, and polishing industries. Cadmium (Cd<sup>2+</sup>) enters the water from electroplating, batteries and photovoltaic cells, fabric factories and metal [7–10]. Chromium (Cr<sup>6+</sup>) causes liver damage, stomach distress and nephritis, and is also responsible for nasal mucous ulcers [11,12]. Zinc (Zn<sup>2+</sup>) enters the water from mining activities and industrial waste. Zinc (Zn<sup>2+</sup>) causes several adverse health effects, e.g., gastrointestinal problems and cardiovascular problems, and can cause DNA damage, resulting in carcinogenic effects and neurotoxicity [13].

Heavy metal ions can be separated from water in several ways: the ion exchange method, precipitation, coagulation, the biosorption method, and the adsorption method [5,14–17].

Adsorption is a process in which the chemicals are accumulated on a solid (adsorbate) surface, and the reverse of this process, where the adsorbed chemicals are detached from the adsorbate, is known as desorption. The removal of heavy metals from water by the adsorption process offers many advantages over other methods, e.g., it is an economical process, it is user-friendly, it has high efficiency, it regenerates the adsorbate, and the adsorbate can easily be regenerated and reused [1,2,8,10,18].

The process of adsorption is affected by various parameters; the dosage of the adsorbate, the solution pH, the concentration of the metal ions and the contact time, etc. [4,5,18]. The increase in the dosage amount of the adsorbate rapidly increases the removal efficiency due to the more significant number of sites available for the attachment of the adsorbent [19]. The pH of the solution has a more significant impact on the adsorption, and the pH is optimized for the maximum adsorption of different adsorbents. Adsorption has many applications, e.g., the treatment of wastewater treatment, gas/air purifier masks, the purification of oil/petroleum products, the separation of gases, the purification of sugar, nitrate adsorption, the softening of water and decolorization, etc. [20].

The activated carbon structure comprises three parts: microcrystalline graphite, amorphous carbon and reticular carbon of a single plane. The activated carbon structure is mainly composed of the microcrystalline graphite structure. However, its structure is different from graphite. The microcrystalline structure of activated carbon possesses interlayer spacing of 0.34–0.35 nm. It cannot be transformed into graphite even if it is heated higher than 2000 °C; that is why it is known as non-graphite microcrystal [21,22]. This microcrystalline structure imparts the porous structure to the activated carbon. The pore size of activated carbon can be divided into three categories based on its diameter; micropores (width < 2 nm), mesopores (width 2–50 nm) and macropores (width > 50 nm) [23,24]. The adsorption efficiency of the activated carbon depends on its physical structure, pore size and chemical structure, i.e., the presence of different functional groups incorporated during the treatment of the parent material before the activation in the furnace. The most common activators used are acidic, alkaline and neutral, imparting different functional groups onto the surface of the adsorbents [25,26]. Activated carbon can be synthesized from various materials containing carbon; agricultural wastes, apricot stones, sewage sludge, waste of the newspapers, and different parts of the plants [27].

Malaysia, Indonesia, Nigeria, African countries, Cameroon and China produce millions of tons of oil palm agricultural waste. Malaysia is one of the top oil palm producers, with about 4.5 million hectares [4,5]. Palm kernel shell (PKS) is a waste of the oil palm upstream industry, is produced in massive amounts, and is disposed of by burning, resulting in environmental pollution and the greenhouse effect. Researchers are trying to utilize the invaluable waste material products and save environmental pollution [4–6,27]. In this study, functionalized activated carbon (FAC) was prepared using PKS as a carbon source. Then, the activated carbon obtained was functionalized by the oxidation with nitric acid followed by washing to remove the excess acid. Furthermore, the resulting FAC was used for the treatment of heavy metal-contaminated water. The prepared FAC was found to be very effective in the purification of heavy metal-contaminated water.

## 2. Materials and Methods

The chemicals used were palm kernel shell (PKS), deionized water with a resistivity of 18 MΩ, phosphoric acid (H<sub>3</sub>PO<sub>4</sub>), stock solutions of Cr<sup>6+</sup>, Cd<sup>2+</sup>, Zn<sup>2+</sup> and Pb<sup>2+</sup>, and nitric acid (HNO<sub>3</sub>) purchased from Sigma Aldrich (St. Louis, MO, USA).

### 2.1. Instrumentation

The instruments used for the characterization of the samples in this work were an FTIR spectrophotometer (Perkin-Elmer 100 series, Waltham, MA, USA), an XRD (Shimadzu, Kyoto, Japan), a Raman spectrometer (WiTec, Ulm, Germany), a field emission scanning electron microscope (FESEM) NOVA NANOSEM 230 model, Denton, TX, USA), an inductively coupled plasma-Optical Emission Spectrometer (ICP-OES), Optima 2100 DV Perkin

Elmer and a BET surface area analyzer (Micromeritics Model: Tristar II Plus) Norcross, GA 30093-USA.

### 2.2. Pretreatment, Activation and Preparation of the Activated Carbon

The PKS samples were collected from a local Palm Oil Mill in Dengkil, Selangor. The PKS sample was cleaned with deionized water, followed by drying at 60 °C in an oven. After the drying, the PKS sample was ground to a powder in an automatic blender and subjected to activation by the treatment with phosphoric acid according to the previously reported method [28]. In brief, for the optimization of the activation, about 20 g of the PKS sample was treated with various concentrations of phosphoric acid: 0%, 5%, 10%, 20%, 30% and 40% (*v/v*) with constant agitation at 120 rpm for one day. The next day, the sample was filtered and dried in an oven at 60 °C. After that, the sample was subjected to a tubular furnace to prepare the activated carbon under a constant nitrogen gas flow at 150 cm<sup>3</sup>/minute. The activated carbon preparation parameters, temperature and holding time were then optimized. The sample treated with 20% phosphoric acid was found to have the highest surface area [28].

### 2.3. Optimization of the Temperature, Holding Time and Functionalization

The temperature for the synthesis of the activated carbon was optimized by putting 5 g of the 20% phosphoric acid-treated PKS sample in a furnace under different temperatures; 500, 600, 700, 800 and 900 °C, with a holding time of 2 h and a heating rate of 10 °C/minutes under an inert environment of an N<sub>2</sub> (g) flow. The holding time was optimized by varying the carbonization time; 1, 2, 3, 4 and 5 h. These conditions were applied to all of the phosphoric acid-treated PKS samples, as reported previously [27,28]. The following are the optimized conditions applied to synthesize the activated carbon; phosphoric acid, 20%; temperature, 500 °C; and a 2 h holding time [29,30]. The activated carbon prepared with the optimized conditions was found to have the highest surface area and was further functionalized with nitric acid (HNO<sub>3</sub>). The functionalization was optimized by treating the sample with different concentrations of nitric acid; 10, 15, 20 and 25%.

Surface Area Analysis: In the BET analysis, N<sub>2</sub> gas was absorbed on the sample surface, and where the pressure was applied, and the volume of the absorbed N<sub>2</sub> gas was measured. The FAC samples were degassed at 290 °C under vacuum for 9 h before the adsorption–desorption measurements were carried out, and we performed the experimental adsorption–desorption measurements. Then, we applied mathematical models for the surface area and porosity analyses [28].

### 2.4. Batch Experiment Set-Up

#### 2.4.1. pH Optimization

The pH for the adsorption studies was optimized by varying the pH of the solution; 2, 3, 4, 5 and 6. Three other parameters were kept constant; a 100 mL solution of each of the metal ions with a concentration of 40 mg/L, an adsorbent dosage of 0.2 g and a contact time of 2 h.

#### 2.4.2. Adsorption Dosage Optimization

The adsorbent dosages were varied; 0.1 g, 0.15 g, 0.2 g and 0.25 g, and all of the other parameters were kept constant; a 100 mL solution of each of the metal ions with a concentration of 40 mg/L, a contact time of 2 h and a pH of 6.

#### 2.4.3. Optimization of the Metal Ion Concentrations

The metal ion concentrations were optimized by varying them; 10, 20, 30, 40 and 50 mg/L in a 100 mL solution and the other three parameters were kept constant; pH 6, a contact time of 2 h and adsorbent dosage of 0.25 g.

#### 2.4.4. Optimization of the Contact Time

The contact time was optimized by varying it; 15, 30, 60, 90 and 120 min. The other three parameters were set; a pH of 6, a concentration of 40 mg/L in a 100 mL solution and an adsorbent dosage of 0.25 g.

### 3. Results and Discussion

#### 3.1. BET Surface Area Analysis

The activated carbon with a surface area of 1099 m<sup>2</sup>/g was selected for the functionalization with percentage concentrations of nitric acid; 10, 15, 20 and 25%. The oxidation with nitric acid resulted in the functionalization of the activated carbon. These FAC samples were subjected to BET analysis to determine their surface area, given in Figure 1. As shown in the figure, the FAC prepared at 15% nitric acid was found to have a maximum surface area of 700 m<sup>2</sup>/g, and this sample was then selected for further parametric optimization.

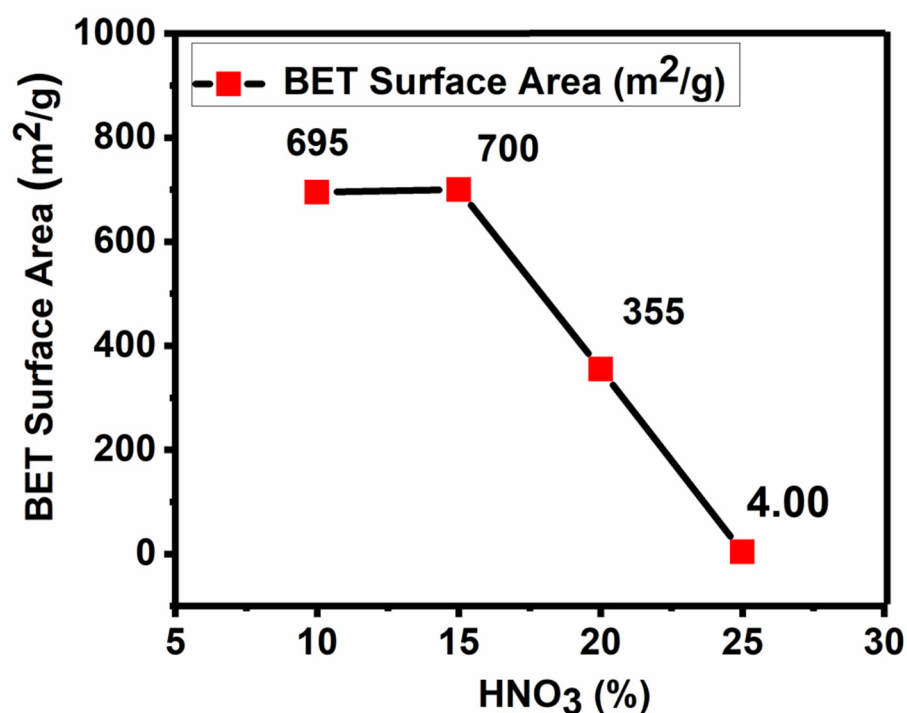
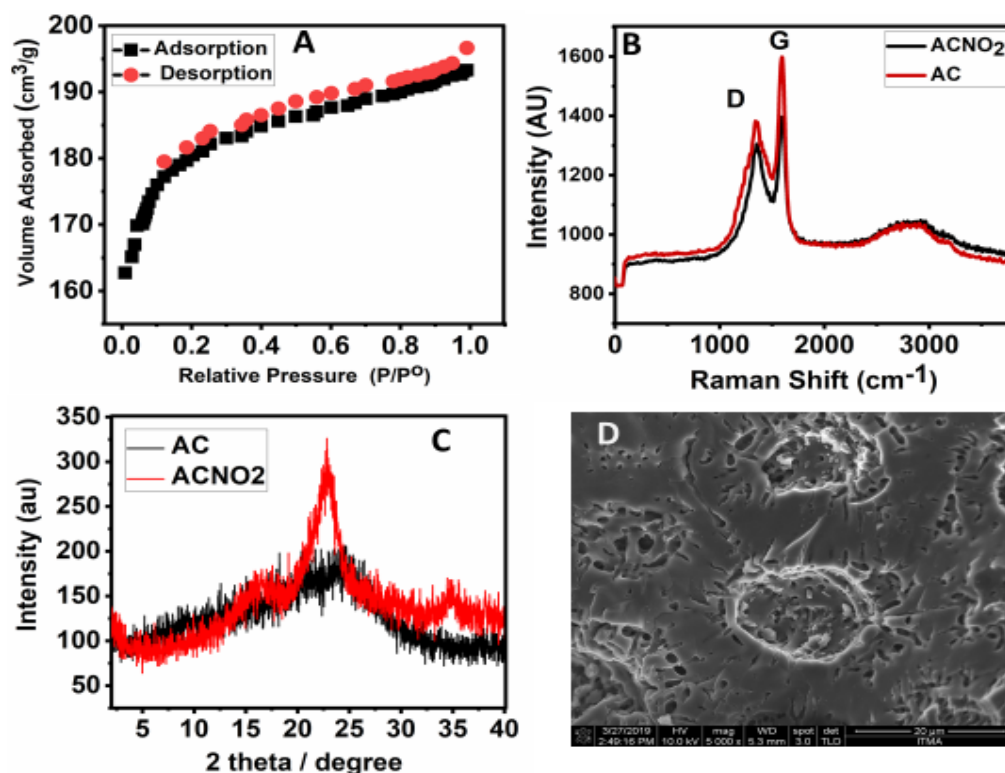


Figure 1. BET Surface area of the FAC prepared at different percentages of nitric acid.

#### 3.2. Adsorption–Desorption Isotherms

The isotherms for the adsorption and desorption for the FAC are shown in Figure 2A, which follows Type I by the IUPAC classification. The Type 1 isotherm of the adsorption and desorption suggests the nanoporous nature of a surface area of 700 m<sup>2</sup>/g for the activated carbon treated with 15% HNO<sub>3</sub>. That sample is termed 'functionalized activated carbon' (FAC). The isotherm is similar to the other activated carbons reported in the literature [27,28].



**Figure 2.** Adsorption—desorption isotherm of FAC (A), Raman spectroscopy of AC and FAC (B), XRD diffraction patterns of AC and FAC (C) and a FESEM micrograph of FAC (D).

### 3.3. Raman Spectroscopic Analysis

Raman spectroscopy is a widely used technique for analyzing different types of carbon-based materials; amorphous carbon, activated carbon, graphite, graphene, graphene oxide and diamond, etc. [29,30]. The Raman bands are associated explicitly with the internal structure; the G band is graphitic sp<sup>2</sup> hybridized carbon, and the D band is related to the disorders/defects in the graphitic structure [28,31,32]. Figure 2B shows the Raman spectra of AC and FAC, where the D and G bands in AC have higher intensity but are relatively lower in FAC. The I<sub>D</sub>/I<sub>G</sub> ratio for AC was found to be 0.86 compared to 0.93 in FAC. The data obtained strongly suggest the successful functionalization of AC with the nitrate group [31,32].

### 3.4. X-ray Diffraction and Surface Morphology

The XRD patterns of activated carbon (Figure 2C) show a hump at 2θ = 5–35, similar to the one reported in the literature [27,28]. The functionalization of activated carbon with the nitrate group resulted in XRD patterns with relatively higher intensity, possibly due to the nitro group bonded on the AC surface, as shown in Figure 2C. It also suggests that the higher crystallinity of FAC compared to AC. Figure 2D shows the surface morphology obtained by the FESEM technique, showing the porous structure of FAC and a similar structure for activated carbon [4,27,28].

### 3.5. Infrared Spectroscopy

Infrared spectroscopy is a valuable technique for the functional group analysis of the samples of interest. Figure 3 shows the FTIR spectra of the FAC before and after the adsorption of the metal ions; Cr<sup>6+</sup>, Pb<sup>2+</sup>, Cd<sup>2+</sup> and Zn<sup>2+</sup>. The FAC sample shows the characteristic functional group bands of C-H, CH<sub>2</sub>, C-N, nitro groups and a C-C bond, etc. [33,34]. These infrared bands of the functional group have been shifted, especially for C=O, N=O and N-O bands, as these functional groups provide the active sites for

the adsorption of metal ions [4,6,27,28]. The slight shifts in the functional groups' bands (Table 1) suggest the successful adsorption of the metal ions on the active sites of the FAC. The metal quantification results from the inductively coupled plasma (ICP) analysis also complement the FTIR results for the adsorption of the metal ions.

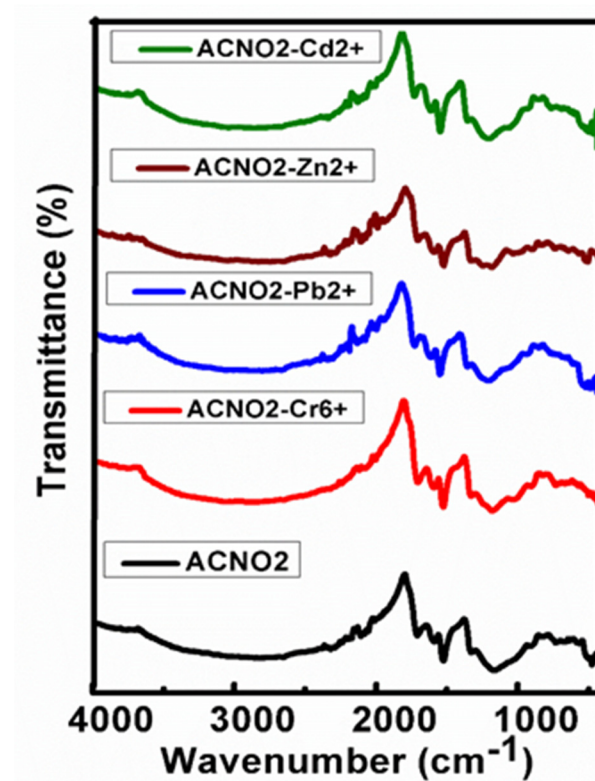


Figure 3. FTIR spectra of FAC before and after the adsorption of the metal ions.

Table 1. Fourier transformed infrared spectroscopic vibrational bands of the different functional groups in FAC before and after the metal ion adsorption.

Assignment	FAC	FAC-Cr <sup>6+</sup>	FAC-Pb <sup>2+</sup>	FAC-Cd <sup>2+</sup>	FAC-Zn <sup>2+</sup>	Reference
V (C-H)	2815	2878	2793	2844	2830	[27,28,33]
C=O	1707	1720	1715	1725	1725	[27,28,33]
N=O	1581	1590	1587	1588	1590	[27,28,33]
	1520	1527	1525	1528	1525	[33,34]
N-O	1328	1331	1327	1327	1336	[33,34]
C-N	1250	1250	1252	1250	1256	[33,34]
	1162	1182	1177	1173	1182	
	1020	1026	1023	1020	1030	
	911	899	900	905	908	[27,33,34]
	837	819	823	818	832	
CH <sub>2</sub> (rocking)	735	733	730	735	734	

### 3.6. Batch Studies

#### 3.6.1. Effect of pH

The pH is the critical parameter in adsorption studies as it has an immense effect on the interaction of metal ions with adsorbents [35]. In this study, the pH was varied up to

6 because, at a higher pH, metal ions may produce precipitation and adsorption results that are not reliable [35]. The overall adsorption of the heavy metal ions  $\text{Cr}^{6+}$ ,  $\text{Cd}^{2+}$  and  $\text{Pb}^{2+}$  was found to be increased with the increase in pH, with the maximum adsorption of almost 100% at pH 6, except for  $\text{Zn}^{2+}$ , which showed the highest adsorption of 70% at pH 5, as shown in Figure 4. This optimized pH was then selected for the remaining batch studies; dosage, concentration and contact time.

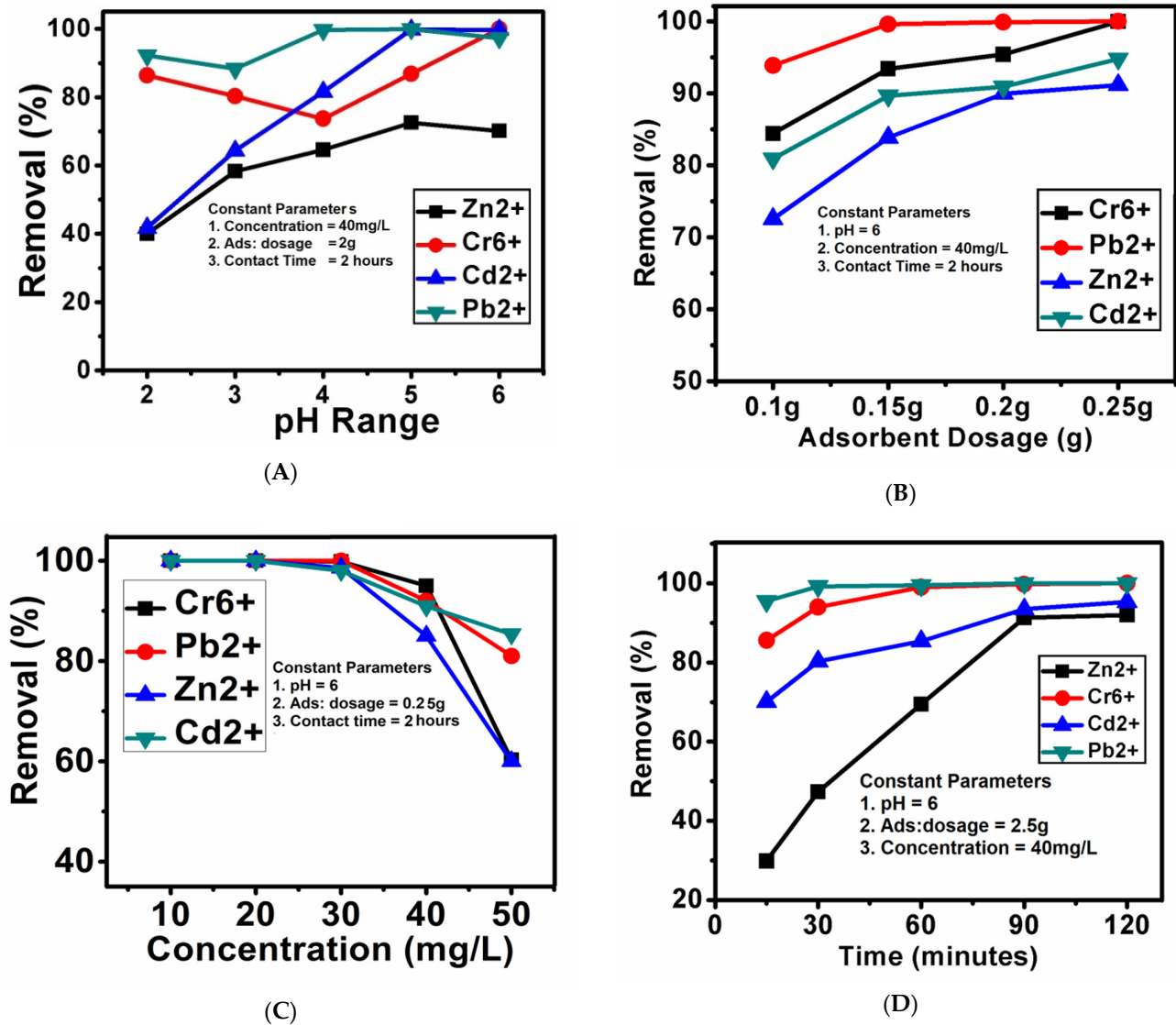


**Figure 4.** (A–D) The effects of different parameters; pH, adsorbent dosage, metal ion concentration and contact time on the percentage removal of the metal ions.

### 3.6.2. Effect of the Adsorbent Dosage

Under the optimized pH condition, the adsorbent dosage was studied by varying the amount of the adsorbent dosage (FAC); 0.1, 0.15 g, 0.2 and 0.25 g, in 100 mL of 40 mg/L heavy metal ion solutions. The adsorption of the heavy metal ions was found to be more than 70% for metal ions, which was increased with the increase in the adsorbent dosage. The metal ions  $\text{Cr}^{6+}$  and  $\text{Pb}^{2+}$  were 100% removed at the adsorbent dosage of 0.25 g, while the metal ions  $\text{Cd}^{2+}$  and  $\text{Pb}^{2+}$  were removed by more than 90%, as shown in Figure 4.

### 3.6.3. Effect of the Metal Ion Concentration

The effect of heavy metal ion concentration was determined by varying their concentrations. Different concentrations of heavy metal ions; 10, 20, 30, 40 and 50 mg/L were used. All four metal ions were found to be 100% removed even up to 30 mg/L, and the adsorption at 40 mg/L was decreased to 95%, 92%, 90% and 85% for  $\text{Cr}^{6+}$ ,  $\text{Pb}^{2+}$ ,  $\text{Cd}^{2+}$  and  $\text{Zn}^{2+}$ , respectively. At the maximum concentration of 50 mg/L, the adsorption was about 85% for three metal ions;  $\text{Cr}^{6+}$ ,  $\text{Pb}^{2+}$  and  $\text{Cd}^{2+}$ . However, the  $\text{Zn}^{2+}$  metal ion adsorption was found to be around 60%. Figure 4 shows the effect of concentration on the adsorption process. Similar adsorption trends for these metal ions have also been reported previously [4,27].

### 3.6.4. Effect of Contact Time

The effect of contact time on the adsorption process was determined by varying the contact times; 15, 30, 60, 90 and 120 min under the previously optimized parameters. The  $\text{Pb}^{2+}$  and  $\text{Cr}^{6+}$  ions showed quick adsorption as more than 80% adsorption took place in the first 15 min and raised to 100% within 60 min.  $\text{Cd}^{2+}$  ions showed better adsorption starting with 70% at 15 min and gradually increasing to above 90% within 120 min. However,  $\text{Zn}^{2+}$  ions took more time for adsorption compared to all of the other three metal ions. They started from 30% initially at 15 min and gradually reached 90% within 120 min. The overall adsorption increased with the increase in contact time between the metal ion solution and the adsorbent.

Previously work on the preparation of activated carbon using PKS materials (non-functionalized activated carbon) as the precursor was reported by Nicholas et al. (2018). The non-functionalized activated carbon was able to remove heavy metal ions;  $\text{Cr}^{6+}$ ,  $\text{Pb}^{2+}$ ,  $\text{Cd}^{2+}$  and  $\text{Zn}^{2+}$  from the simulated aqueous solution up to concentrations of 15 mg/L [27]. In another study, Mohibullah et al. (2020) synthesized activated carbon from *Albizia lebbek* and *Melia azedarach* trees and applied them to remove  $\text{Pb}^{2+}$  and  $\text{Cd}^{2+}$  metal ions from an aqueous solution [36]. They found that the activated carbon of *Albizia lebbek* trees removed 75% of the  $\text{Pb}^{2+}$  and 77% of the  $\text{Cd}^{2+}$  from a 100 mL solution with a concentration of 40 mg/L. They also applied the activated carbon of the *Melia azedarach* tree to remove these two metal ions under the above identical conditions. They found that the activated carbon removed 62% and 66% of the  $\text{Pb}^{2+}$  and  $\text{Cd}^{2+}$ , respectively [36].

Shahrokhi et al. (2021) synthesized activated carbon from pulverized tire waste and used it to remove  $\text{Pb}^{2+}$ ,  $\text{Cu}^{2+}$  and  $\text{Zn}^{2+}$  metal ions. The adsorption capacities were found to be 322.5, 185.2 and 71.9  $\text{mg}\cdot\text{g}^{-1}$  for  $\text{Pb}^{2+}$ ,  $\text{Cu}^{2+}$  and  $\text{Zn}^{2+}$ , respectively. Furthermore, the adsorption was fitted well with the pseudo-second-order kinetics [37]. Zaini et al. (2021) activated the pore texture of fiber-based activated carbon and applied it to remove  $\text{Cu}^{2+}$  and  $\text{Pb}^{2+}$ . The material was able to remove 50% of the  $\text{Cu}^{2+}$  and 75% of the  $\text{Pb}^{2+}$  from a 50 mL aqueous solution with a concentration of 20 mg/L  $\text{Cu}^{2+}$  and 40 mg/L  $\text{Pb}^{2+}$  [38]. Vishnu et al. (2020) impregnated activated carbon with biosynthesized melanin and applied it to remove heavy metals;  $\text{Hg}^{2+}$ ,  $\text{Cr}^{6+}$ ,  $\text{Pb}^{2+}$  and  $\text{Cu}^{2+}$  from an aqueous solution [39]. The melanin-impregnated activated carbon was found to removed 84.59%  $\text{Hg}^{2+}$ , 86.6%  $\text{Cr}^{6+}$ , 91.1%  $\text{Pb}^{2+}$  and 93.8%  $\text{Cu}^{2+}$ , bypassing the 5 mg/L heavy metal solution from the column packed with melanin-impregnated activated carbon [39]. Li et al. (2018) p thiol-functionalized activated carbon from sewage sludge and used it for heavy metal removal from aqueous solutions. The synthesized thiol-functionalized activated carbon showed adsorption capacities for  $\text{Cu}^{2+}$ ,  $\text{Pb}^{2+}$ ,  $\text{Cd}^{2+}$  and  $\text{Ni}^{2+}$  of 238.1, 96.2, 87.7 and 52.4 mg/g, respectively. Furthermore, the Langmuir model was fitted well with the adsorption of these metal ions [40]. The functionalized activated carbon designed in this study showed a better removal percentage for  $\text{Cr}^{6+}$ ,  $\text{Pb}^{2+}$ ,  $\text{Cd}^{2+}$  and  $\text{Zn}^{2+}$ . Moreover, the kinetics and isotherm models are described in detail in this study.

### 3.7. Kinetics of the Metal Ion Adsorption

The kinetic studies of the heavy metal ion adsorption on the functionalized activated carbon were determined by applying different kinetics models, namely the pseudo-first-order, pseudo-second-order and parabolic diffusion.

The pseudo-first-order equation, in its linear form, is written as follows:

$$\ln (q_e - q_t) = \ln q_e - k_1 t \quad (1)$$

where  $q_e$  represents the adsorption equilibrium,  $q_t$  is adsorption at any time  $t$ , and  $k$  is the rate constant that can be determined by obtaining the slope by plotting  $\ln (q_e - q_t)$  versus  $t$ .

The linear equation for the pseudo-second-order can be written as follows:

$$t/q_t = 1/k_2 q_e^2 + t/q_e \quad (2)$$

The equation for parabolic diffusion is written as follows:

$$1 - (M_t/M_0)/t = Kt^{-0.5} + b \quad (3)$$

where the adsorption at time 0 and at time  $t$  is represented by  $M_0$  and  $M_t$ , respectively, in the above equations [4,41,42]. Table 2 contains the detailed parameters of all three kinetic adsorption models.

**Table 2.** Kinetic models and their detailed parameters.

Kinetic Model	Parameters
Pseudo-first-order	$q_e$ = adsorption equilibrium $q_t$ = adsorption at time $t$ $k_1$ = rate constant for pseudo-first-order $\ln$ = natural log
Pseudo-second-order	$q_e$ = adsorption equilibrium $q_t$ = Adsorption at time $t$ $k_2$ = Rate constant for Psudo second Order
Parabolic-Diffusion	$M_0 = q_e$ $M_t = (q_e - q_t)/q_e$ $t^{0.5}$ = at half time $K$ = the adsorption constant

Figure 5 shows the kinetic fitting for the adsorption of heavy metal ions on FAC using the pseudo-first-order, pseudo-second-order and parabolic diffusion models. The adsorption of the heavy metal ions;  $Cr^{6+}$ ,  $Cd^{2+}$ ,  $Pb^{2+}$  and  $Zn^{2+}$  on FAC were found to follow the pseudo-second-order model. The correlation coefficient,  $R^2$  was found to be 0.9999 for the pseudo-second-order fitting for the adsorption of heavy metal ions on FAC. Similar kinetics fittings have been reported in the literature [4,27]. The adsorption process that follows the pseudo-second-order kinetics is said to involve chemisorption interactions [4,30,43,44].

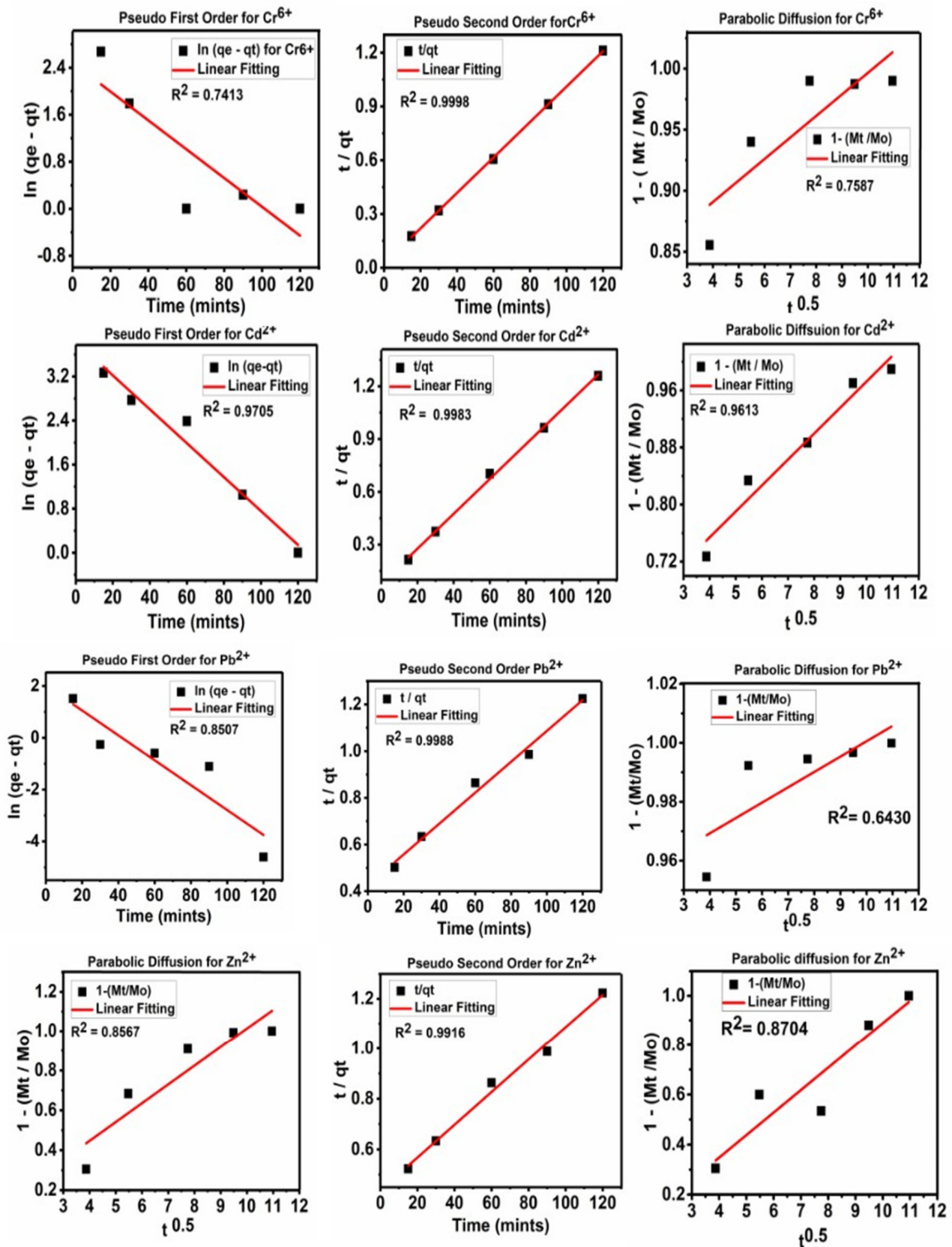


Figure 5. The kinetic fitting for the pseudo-first-order, pseudo-second-order and parabolic-diffusion models for the adsorption of the heavy metal ions;  $\text{Cr}^{6+}$ ,  $\text{Cd}^{2+}$ ,  $\text{Pb}^{2+}$  and  $\text{Zn}^{2+}$  on FAC.

#### 4. Adsorption Isotherms

The Langmuir and Freundlich isotherms were applied to determine the interaction between the metal ions;  $\text{Cr}^{6+}$ ,  $\text{Pb}^{2+}$ ,  $\text{Cd}^{2+}$  and  $\text{Zn}^{2+}$  and the adsorbent, functionalized activated carbon (FAC). Equation (4) represents the Langmuir isotherm followed by Equation (5) for its straight line. Equation (6) represents the Freundlich isotherm, followed by its straight-line Equation (7).

$$Q_e = (b Q_m C_e) / (1 + b C_e) \quad (4)$$

Linear form

$$C_e / q_e = (C_e / q_m) + 1 / b q_m \quad (5)$$

$$Q_{eq} = k_f \times C_{eq} \times 1/n \quad (6)$$

Linear form

$$\text{Log } q_e = \text{log } K_f + 1/n \times \text{log } C_e \quad (7)$$

In the above equations,  $C_e$  and  $Q_e$  represent the metal ion concentration (mg/L) at equilibrium and the quantity of the metal ions adsorbed (mg/g) on the adsorbent, FAC.  $Q_m$  represents the metal ions adsorbed (mg/g) on the adsorbent, FAC, and  $b$  is a constant. The terms  $K_f$  and  $1/n$  are Freundlich coefficients.

Figure 6 shows the fitting of the adsorption for the Freundlich and Langmuir isotherm models. Table 3 shows the correlation coefficients ( $R^2$ ) and the values of the constants of the Langmuir and Freundlich isotherms for the  $\text{Cr}^{6+}$ ,  $\text{Cd}^{2+}$ ,  $\text{Zn}^{2+}$  and  $\text{Pb}^{2+}$  metal ion adsorption of FAC. The maximum adsorption for the metal ions  $\text{Cr}^{6+}$  and  $\text{Pb}^{2+}$  was found to be 40 mg/g and 38 mg/g, and 37 mg/g for both  $\text{Cd}^{2+}$  and  $\text{Zn}^{2+}$ , respectively. The isotherm analysis revealed that the adsorption of  $\text{Cr}^{6+}$ ,  $\text{Cd}^{2+}$ ,  $\text{Zn}^{2+}$  and  $\text{Pb}^{2+}$  follow the Freundlich isotherm model, as their correlation coefficient is higher than that of the Langmuir shown in Table 3. The adsorption that follows the Freundlich models suggests that the active adsorbent sites of FAC are uniformly distributed over the surface and that the metal ions are adsorbed onto the surface [4,35]. The Freundlich  $n_f$  constant values for the metal ion adsorption were found to be between 0.1 and 1, which suggests the favorable adsorption of metal ions on FAC.

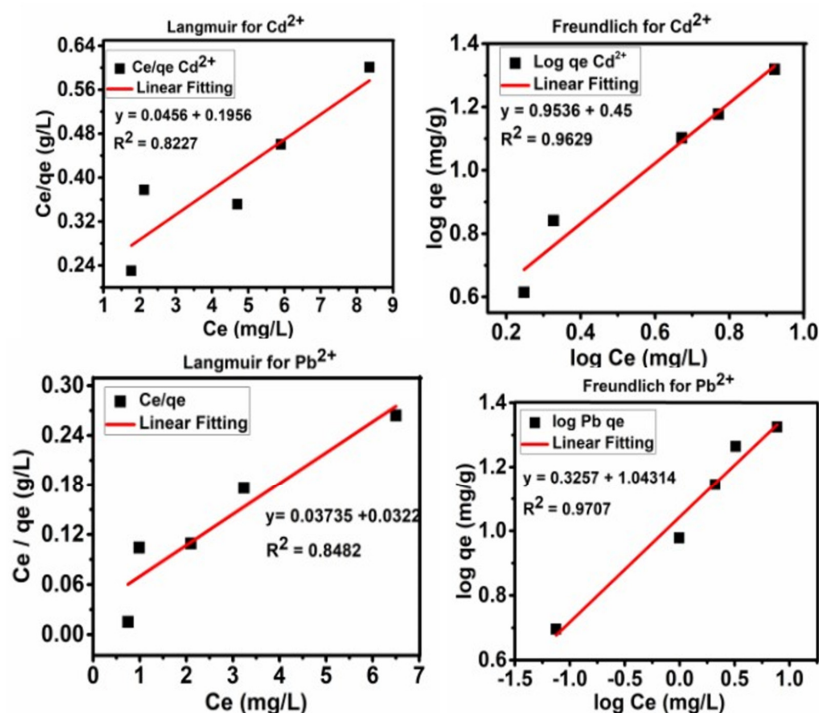
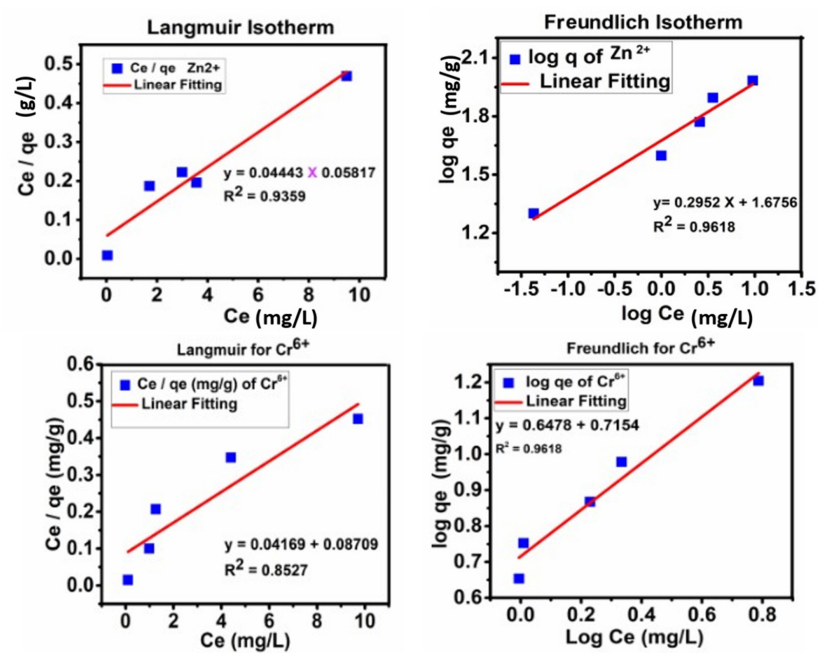


Figure 6. Cont.



**Figure 6.** The Langmuir and Freundlich isotherms for the adsorption of  $\text{Cr}^{6+}$ ,  $\text{Cd}^{2+}$ ,  $\text{Pb}^{2+}$  and  $\text{Zn}^{2+}$  on FAC.

**Table 3.** Correlation coefficients ( $R^2$ ) and constants for the Langmuir and Freundlich isotherms for  $\text{Pb}^{2+}$ ,  $\text{Cd}^{2+}$ ,  $\text{Zn}^{2+}$  and  $\text{Cr}^{6+}$  adsorption on FAC.

Metal Ion	Langmuir Isotherm			Freundlich Isotherm		
	$q_e$ (mg/g)	$b$ (L/mg)	$R^2$	$K_f$	$n_f$	$R^2$
$\text{Cd}^{2+}$	38	0.04	0.82	0.95	0.45	0.96
$\text{Pb}^{2+}$	40	0.03	0.84	0.32	1.04	0.97
$\text{Zn}^{2+}$	37	0.04	0.93	0.29	1.60	0.96
$\text{Cr}^{6+}$	40	0.04	0.85	0.64	0.71	0.96

## 5. Adsorption Capacity

The adsorption capacity is the amount of metal ions (mg) adsorbed on the adsorbent, FAC, in grams over different time intervals. The adsorption capacity was determined by keeping constant the metal ion concentration at 100 mL of 40 mg/L solutions and 0.25 g of the adsorbent, FAC. Figure 7 shows the adsorption capacity of FAC for different metal ions concerning the contact time. It can be seen that  $\text{Pb}^{2+}$  ions showed faster adsorption, taking only 30 min for the maximum adsorption of 40 mg/g, followed by  $\text{Cr}^{6+}$ , which took 60 min for the maximum adsorption of 40 mg/g.  $\text{Cd}^{2+}$  ions showed an adsorption capacity starting from 27 mg/g at 15 min and reaching saturation at 38 mg/g in 120 min. The metal ion,  $\text{Zn}^{2+}$ , started from the lowest adsorption of 12 mg/g and gradually reached the maximum adsorption (saturation) at 37 mg/g in 120 min. The maximum adsorption ( $q_e$ ) for each metal ion is given in Table 3.

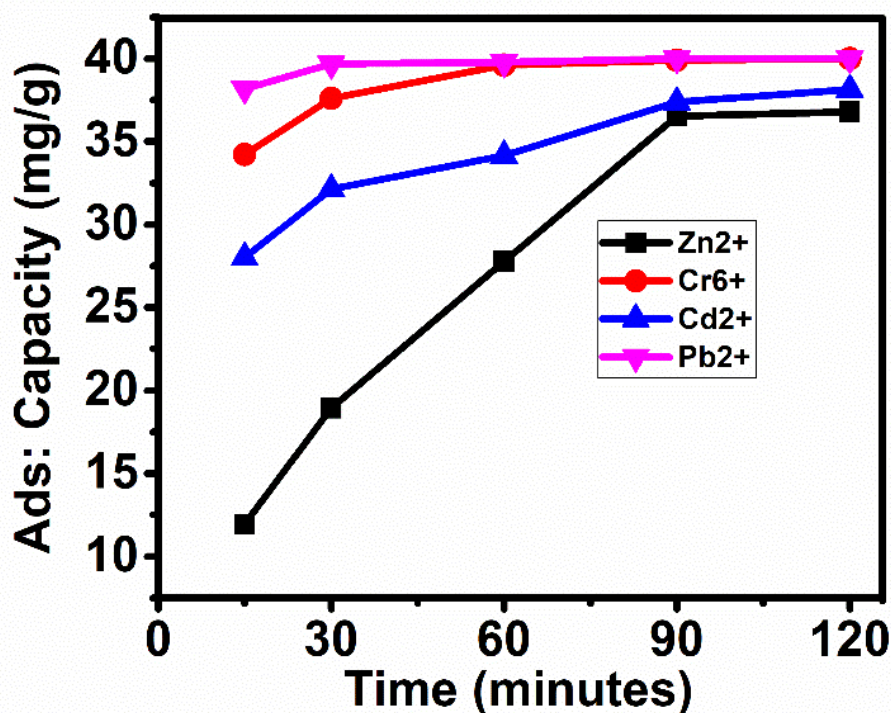


**Figure 7.** Adsorption capacities ( $q_e$ ) of FAC at different time intervals for the adsorption of metal ions; Zn<sup>2+</sup>, Cr<sup>6+</sup>, Pb<sup>2+</sup> and Cd<sup>2+</sup>.

## 6. Conclusions

In this study, functionalized activated carbon was prepared using phosphoric acid as a chemical activator, and nitric acid was used to functionalize the activated carbon. The resulting FAC was found to contain a high surface area of 700 m<sup>2</sup>/g. The BET adsorption-desorption isotherms suggested the porous nature of the AC. The FTIR results suggested the successful functionalization of the activated carbon. The FAC took 90 min for the maximum adsorption of about 100% for Cr<sup>6+</sup> and Pb<sup>2+</sup>, and about 90% adsorption for the Cd<sup>2+</sup> and Zn<sup>2+</sup> with the original concentration of 40 mg/L. The kinetic studies suggested that the adsorption follows the pseudo-second-order model, and the adsorption isotherms revealed that the adsorption follows the Freundlich model. This study is a greener approach to the preparation of a useful functionalized activated carbon (FAC) from agricultural waste, i.e., palm kernel shells, and the resulting FAC can be applied for environmental remediation, i.e., the treatment of heavy metal-contaminated water. Apart from environmental remediation, the FAC can be used in other technological applications such as biomedical applications and thermal energy storage, etc.

**Author Contributions:** Conceptualization, R.B. and M.Z.H.; methodology, R.B., M.Z.H., Z.Z., and A.H.A.; software, R.B. and M.Z.H.; validation, R.B., M.Z.H., Z.Z. and A.H.A.; formal analysis, R.B. and M.Z.H.; investigation, R.B. and M.Z.H.; resources, R.B., M.Z.H., Z.Z. and A.H.A.; data curation, R.B. and M.Z.H.; writing—original draft preparation, R.B. and M.Z.H.; writing—review and editing R.B. and M.Z.H.; visualization, R.B.; supervision, M.Z.H., Z.Z. and A.H.A.; project administration, M.Z.H.; funding acquisition, M.Z.H. All authors have read and agreed to the published version of the manuscript.

**Funding:** Universiti Putra Malaysia and the Ministry of Higher Education of Malaysia funded this project under UPM/800-3/3/1/GBP/2019/9678800.

**Institutional Review Board Statement:** Not applicable.

**Informed Consent Statement:** Not applicable.

**Data Availability Statement:** Not applicable.

**Acknowledgments:** The authors greatly acknowledge the technical staff of the Material Synthesis and characterization laboratory, Institute of Advanced Technology, Universiti Putra Malaysia.

**Conflicts of Interest:** The authors declare no conflict of interest.

## References

1. Yang, Z.-Z.; Zhang, C.; Zeng, G.-M.; Tan, X.-F.; Wang, H.; Huang, D.-L.; Yang, K.-H.; Wei, J.-J.; Ma, C.; Nie, K. Design and engineering of layered double hydroxide based catalysts for water depollution by advanced oxidation processes: A review. *J. Mater. Chem. A* **2020**, *8*, 4141–4173. [[CrossRef](#)]
2. Shi, X.; Ding, Z.; Wang, C.; Song, S.; Zhou, X. Effect of different cellulose polymers on the crystal growth of celecoxib polymorphs. *J. Cryst. Growth* **2020**, *539*, 125638. [[CrossRef](#)]
3. Ali, H.; Khan, E.; Ilahi, I. Environmental Chemistry and Ecotoxicology of Hazardous Heavy Metals: Environmental Persistence, Toxicity, and Bioaccumulation. *J. Chem.* **2019**, *2019*, 1–14. [[CrossRef](#)]
4. Baby, R.; Saifullah, B.; Hussein, M.Z. Palm Kernel Shell as an effective adsorbent for the treatment of heavy metal contaminated water. *Sci. Rep.* **2019**, *9*, 18955. [[CrossRef](#)] [[PubMed](#)]
5. Baby, R.; Saifullah, B.; Hussein, M.Z. Carbon Nanomaterials for the Treatment of Heavy Metal-Contaminated Water and Environmental Remediation. *Nanoscale Res. Lett.* **2019**, *14*, 341. [[CrossRef](#)]
6. Baby Shaikh, R.; Saifullah, B.; Rehman, F.U. Greener Method for the Removal of Toxic Metal Ions from the Wastewater by Application of Agricultural Waste as an Adsorbent. *Water* **2018**, *10*, 1316. [[CrossRef](#)]
7. Cooper, A.M.; Felix, D.; Alcantara, F.; Zaslavsky, I.; Work, A.; Watson, P.L.; Pezzoli, K.; Yu, Q.; Zhu, D.; Scavo, A.J.; et al. Monitoring and mitigation of toxic heavy metals and arsenic accumulation in food crops: A case study of an urban community garden. *Plant Direct* **2020**, *4*, e00198. [[CrossRef](#)] [[PubMed](#)]
8. El-Dib, F.I.; Mohamed, D.E.; El-Shamy, O.A.A.; Mishrif, M.R. Study the adsorption properties of magnetite nanoparticles in the presence of different synthesized surfactants for heavy metal ions removal. *Egypt. J. Pet.* **2020**, *29*, 1–7. [[CrossRef](#)]
9. Li, Z.; Wang, L.; Meng, J.; Liu, X.; Xu, J.; Wang, F.; Brookes, P. Zeolite-supported nanoscale zero-valent iron: New findings on simultaneous adsorption of Cd(II), Pb(II), and As(III) in aqueous solution and soil. *J. Hazard. Mater.* **2018**, *344*, 1–11. [[CrossRef](#)]
10. Liu, X.; Xu, X.; Dong, X.; Park, J. Competitive Adsorption of Heavy Metal Ions from Aqueous Solutions onto Activated Carbon and Agricultural Waste Materials. *Pol. J. Environ. Stud.* **2019**, *29*, 749–761. [[CrossRef](#)]
11. Bansal, N. Industrial Development and Challenges of Water Pollution in Coastal Areas: The Case of Surat, India. *IOP Conf. Ser. Earth Environ. Sci.* **2018**, *120*, 012001. [[CrossRef](#)]
12. Baruthio, F. Toxic effects of chromium and its compounds. *Biol. Trace Element Res.* **1992**, *32*, 145–153. [[CrossRef](#)] [[PubMed](#)]
13. Sankhla, M.S.; Kumar, R.; Prasad, L. Zinc Impurity in Drinking Water and Its Toxic Effect on Human Health. *Indian Internet J. Forensic Med. Toxicol.* **2019**, *17*, 4. [[CrossRef](#)]
14. Ahmed, M.J. Application of agricultural based activated carbons by microwave and conventional activations for basic dye adsorption: Review. *J. Environ. Chem. Eng.* **2016**, *4*, 10. [[CrossRef](#)]
15. Jang, S.; Song, S.; Lim, J.H.; Kim, H.S.; Phan, B.T.; Ha, K.-T.; Park, S.; Park, K.H. Application of Various Metal-Organic Frameworks (MOFs) as Catalysts for Air and Water Pollution Environmental Remediation. *Catalysts* **2020**, *10*, 195. [[CrossRef](#)]
16. Katoch, A.; Goyal, N.; Gautam, S. Applications and advances in coordination cages: Metal-Organic Frameworks. *Vacuum* **2019**, *167*, 287–300. [[CrossRef](#)]
17. Namasivayam, S.K.R.; Kumar, S.N.; Kamil, T.M.; Ravi, T. Biopolymer-Mediated Coating Influence on Wastewater Treatment Efficacy of Silver Nanoparticles Synthesized from Fungal Consortium. *Natl. Acad. Sci. Lett.* **2020**, *43*, 557–561. [[CrossRef](#)]
18. Yuan, J.; Mohamadi, A. Study the adsorption process of 5-Fluorouracil drug on the pristine and doped graphdiyne nanosheet. *J. Mol. Model.* **2021**, *27*, 1–9. [[CrossRef](#)]
19. Hamzadeh, A.; Rashtbari, Y.; Afshin, S.; Morovati, M.; Vosoughi, M. Application of low-cost material for adsorption of dye from aqueous solution. *Int. J. Environ. Anal. Chem.* **2020**, *2020*, 1–16. [[CrossRef](#)]
20. Vilardi, G.; Bubbico, R.; Di Palma, L.; Verdone, N. Nitrate green removal by fixed-bed columns packed with waste biomass: Modelling and friction parameter estimation. *Chem. Eng. Res. Des.* **2020**, *154*, 250–261. [[CrossRef](#)]
21. Negara, D.N.K.P.; Nindhia, T.G.T.; Surata, I.W.; Hidajat, F.; Sucipta, M. Textural characteristics of activated carbons derived from tabah bamboo manufactured by using H<sub>3</sub>PO<sub>4</sub> chemical activation. *Mater. Today Proc.* **2020**, *22*, 148–155. [[CrossRef](#)]
22. Ekpete, O.A.; Marcus, A.C.; Osi, V. Preparation and Characterization of Activated Carbon Obtained from Plantain (*Musa paradisiaca*) Fruit Stem. *J. Chem.* **2017**, *2017*, 8635615. [[CrossRef](#)]
23. Lu, Z.; Sun, W.; Li, C.; Cao, W.; Jing, Z.; Li, S.; Ao, X.; Chen, C.; Liu, S. Effect of granular activated carbon pore-size distribution on biological activated carbon filter performance. *Water Res.* **2020**, *177*, 115768. [[CrossRef](#)]
24. Lei, B.; Xie, H.; Chen, S.; Liu, B.; Zhou, G. Control of pore structure and surface chemistry of activated carbon derived from waste *Zanthoxylum bungeanum* branches for toluene removal in air. *Environ. Sci. Pollut. Res.* **2020**, *27*, 27072–27092. [[CrossRef](#)] [[PubMed](#)]
25. Ruiz-Rosas, R.; García-Mateos, F.J.; Gutiérrez, M.d.C.; Rodríguez-Mirasol, J.; Cordero, T. About the Role of Porosity and Surface Chemistry of Phosphorus-Containing Activated Carbons in the Removal of Micropollutants. *Front. Mater.* **2019**, *6*. [[CrossRef](#)]

26. Khamkeaw, A.; Asavamongkolkul, T.; Perngyai, T.; Jongsomjit, B.; Phisalaphong, M. Interconnected Micro, Meso, and Macro Porous Activated Carbon from Bacterial Nanocellulose for Superior Adsorption Properties and Effective Catalytic Performance. *Molecules* **2020**, *25*, 4063. [[CrossRef](#)] [[PubMed](#)]
27. Baby, R.; Hussein, M.Z. Ecofriendly Approach for Treatment of Heavy-Metal-Contaminated Water Using Activated Carbon of Kernel Shell of Oil Palm. *Materials* **2020**, *13*, 2627. [[CrossRef](#)]
28. Nicholas, A.F.; Hussein, M.Z.; Zainal, Z.; Khadiran, T. Palm Kernel Shell Activated Carbon as an Inorganic Framework for Shape-Stabilized Phase Change Material. *Nanomaterials* **2018**, *8*, 689. [[CrossRef](#)]
29. Lazzarini, A.; Piovano, A.; Pellegrini, R.; Agostini, G.; Rudić, S.; Lamberti, C.; Groppo, E. Graphitization of Activated Carbons: A Molecular-level Investigation by INS, DRIFT, XRD and Raman Techniques. *Phys. Procedia* **2016**, *85*, 20–26. [[CrossRef](#)]
30. Chen, C.-J.; Zhu, W.; Chao, J.-H.; Shang, A.; Lee, Y.G.; Liu, R.; Yin, S.; Dubinskii, M.; Hoffman, R.C. Study of thermal and spatial dependent electric field-induced phase transition in relaxor ferroelectric crystals using Raman spectroscopy. *J. Alloys Compd.* **2019**, *804*, 35–41. [[CrossRef](#)]
31. Murillo Pulgarín, J.A.; Alañón Molina, A.; Jiménez García, E.; García Gómez, L. A sensitive resonance Rayleigh scattering sensor for dopamine in urine using upconversion nanoparticles. *J. Raman Spectrosc.* **2020**, *51*, 406–413. [[CrossRef](#)]
32. Bock, P.; Nousiainen, P.; Elder, T.; Blaukopf, M.; Amer, H.; Zirbs, R.; Potthast, A.; Gierlinger, N. Infrared and Raman spectra of lignin substructures: Dibenzodioxocin. *J. Raman Spectrosc.* **2020**, *51*, 422–431. [[CrossRef](#)] [[PubMed](#)]
33. *Wiley's Solomons, Fryhle & Snyder's Organic Chemistry*, 11th ed.; Yee, J. Ed.; Wiley: Hoboken, NJ, USA, 2018; 1139p.
34. Donald LPavia, G.M.L.; Kriz, G.S.; Vyvyan, J.R. *Introduction to Spectroscopy*, 4th ed.; Brooks/Cole Cengage Learning: Boston, MA, USA, 2009.
35. Egbosiuba, T.C.; Abdulkareem, A.S.; Kovo, A.S.; Afolabi, E.A.; Tijani, J.O.; Bankole, M.T.; Bo, S.; Roos, W.D. Adsorption of Cr(VI), Ni(II), Fe(II) and Cd(II) ions by KIAgNPs decorated MWCNTs in a batch and fixed bed process. *Sci. Rep.* **2021**, *11*, 75. [[CrossRef](#)]
36. Ullah, M.; Nazir, R.; Khan, M.; Khan, W.; Shah, M.; Afridi, S.G.; Zada, A. The effective removal of heavy metals from water by activated carbon adsorbents of Albizia lebbek and Melia azedarach seed shells. *Soil Water Res.* **2019**, *15*, 8. [[CrossRef](#)]
37. Shahrokhi-Shahraki, R.; Benally, C.; El-Din, M.G.; Park, J. High efficiency removal of heavy metals using tire-derived activated carbon vs commercial activated carbon: Insights into the adsorption mechanisms. *Chemosphere* **2021**, *264*, 128455. [[CrossRef](#)] [[PubMed](#)]
38. Zaini, M.A.A.; Zhi, L.L.; Hui, T.S.; Amano, Y.; Machida, M. Effects of physical activation on pore textures and heavy metals removal of fiber-based activated carbons. *Mater. Today Proc.* **2021**, *39*, 917–921. [[CrossRef](#)]
39. Manirethan, V.; Balakrishnan, R.M. Batch and continuous studies on the removal of heavy metals using biosynthesized melanin impregnated activated carbon. *Environ. Technol. Innov.* **2020**, *20*, 101085. [[CrossRef](#)]
40. Li, J.; Xing, X.; Li, J.; Shi, M.; Lin, A.; Xu, C.; Zheng, J.; Li, R. Preparation of thiol-functionalized activated carbon from sewage sludge with coal blending for heavy metal removal from contaminated water. *Environ. Pollut.* **2018**, *234*, 677–683. [[CrossRef](#)]
41. Zhong, Q.; Jin, M. Nanoscale Structures of Spray-Dried Zein Microcapsules and in Vitro Release Kinetics of the Encapsulated Lysozyme As Affected by Formulations. *J. Agric. Food Chem.* **2009**, *57*, 3886–3894. [[CrossRef](#)]
42. McKay, G. The adsorption of dyestuffs from aqueous solutions using the activated carbon adsorption model to determine breakthrough curves. *Chem. Eng. J.* **1984**, *28*, 95–104. [[CrossRef](#)]
43. Ammari, A.; Schroen, K. Flavor Retention and Release from Beverages: A Kinetic and Thermodynamic Perspective. *J. Agric. Food Chem.* **2018**, *66*, 9869–9881. [[CrossRef](#)] [[PubMed](#)]
44. Redman, Z.C.; Tran, K.H.; Parikh, S.J.; Tjeerdema, R.S. Influence of pH and Divalent Metals Relevant to California Rice Fields on the Hydroxide-Mediated Hydrolysis of the Insecticide Chlorantraniliprole. *J. Agric. Food Chem.* **2019**, *67*, 12402–12407. [[CrossRef](#)] [[PubMed](#)]